**Title:** Land cover change during a period of extensive landscape restoration in Ningxia Hui Autonomous Region, China (1980-2015)

**Running head:** Environmental change in NHAR

**List of authors:** Angela M. Cadavid Restrepo[1*], Yu Rong Yang[2,3], Nicholas A.S. Hamm[4], Darren J. Gray[1,3], Tamsin S. Barnes[5,6], Gail M. Williams[7], Ricardo J. Soares Magalhães[5,8], Donald P. McManus[3], Danhuai Guo[9], Archie C.A. Clements[1]

**Institute or laboratory of origin:**

[1] The Australian National University, Research School of Population Health, New South Wales, Australia

[2] Yinchuan, Ningxia Hui Autonomous Region, Ningxia Medical University, P. R. China

[3] QIMR Berghofer Medical Research Institute, Molecular Parasitology Laboratory, Queensland, Australia

[4] University of Twente, Faculty of Geo-Information Science and Earth Observation (ITC), Enschede, The Netherlands

[5] The University of Queensland, School of Veterinary Science, Queensland, Australia

[6] The University of Queensland, Queensland Alliance for Agriculture and Food Innovation, Queensland, Australia

[7] The University of Queensland, Brisbane, School of Public Health, Queensland, Australia

[8] Queensland Children's Medical Research Institute, Children's Health and Environment Program, The University of Queensland, Brisbane, Queensland, Australia

[9] Chinese Academy of Sciences, Computer Network Information Center, Beijing, China

**Corresponding author:** Angela M. Cadavid Restrepo, QIMR Berghofer Medical Research Institute, 300 Herston Rd, Herston, Brisbane, Queensland 4006, Australia, tel. +61 7 3362 0222, fax + 61 7 3362 0104, e-mail: angela.cadavid@anu.edu.au

**Keywords:** environmental change, climate change, land use and land cover change, geographic information systems, remote sensing, Landsat, Ningxia Hui Autonomous region, Earth observations.

**Paper type:** primary research

**Abstract**

Environmental change has been a topic of great interest over the last century due to its potential impact on ecosystem services that are fundamental for sustainable development and human well-being. Here, we assess and quantify the spatial and temporal variation in land cover and climate in Ningxia Hui Autonomous Region (NHAR), China. With high-resolution (30 m) imagery from Landsat 4/5-TM and 8-OLI for the entire region, land cover maps of the region were created to explore local land cover changes in a spatially explicit way. We also collected meteorological data for the period January 1980 to December 2013 to quantify, describe and map climate trends in the Autonomous Region. The results suggest that land cover changes observed in NHAR from 1990 to 2015 reflect the main goals of a national policy implemented there to recover degraded landscapes. Forest, herbaceous vegetation and cultivated land increased by approximately 410,200 ha, 708,600 ha and 164,300 ha, respectively. The largest relative land cover change over the entire study period was the increase in forestland. Forest growth resulted mainly from the conversion of herbaceous vegetation (53.8%) and cultivated land (30.8%). The results also indicate statistically significant positive trends in annual, summer and winter temperatures in most of the region. Statistically significant upward trends in annual and summer precipitation were observed in the northern and central part of the Autonomous Region, whereas significant negative precipitation trends were found in the south. Winter precipitation exhibited the opposite spatial distribution. Accurate information on the local patterns of land cover and climate change in NHAR may contribute to the future establishment of better landscape policies for ecosystem management and protection. Spatially explicit information on environmental change may also help decision makers to understand and respond appropriately to emerging environmental risks for the local population.

## Introduction

Changes in land use and land cover (LULC) are fundamental components of environmental change, and are major determinants of sustainable development and human adaptation to global change (B. L. Turner, Lambin, & Reenberg, 2007; I. Turner, Moss, & Sz Skole). Land cover (biophysical attributes of the land surface) and land use (the purpose for which humans exploit land cover) are of great significance in maintaining the structure and productivity of ecological systems (Lambin et al., 2001). LULC change influences the climate system through effects on the Earth's surface albedo (the fraction of incident electromagnetic radiation reflected by the land surface) and the exchange of greenhouse gases between the soil and the atmosphere (Foley et al., 2005; Roger A Pielke et al., 2002). Thus, land cover change has the potential to impact on climate change at local and regional scales (de Noblet-Ducoudré et al., 2012; Kalnay & Cai, 2003) and also at a global scale (Foley et al., 2005). Extensive LULC change also contributes to soil erosion, simplification of the agricultural landscape and loss or fragmentation of natural habitats (Blaikie & Brookfield, 2015; Bommarco, Kleijn, & Potts, 2013). These effects degrade biodiversity (Newbold et al., 2015; Sala et al., 2000) to such an extent that the well-being and vulnerability of humans to social and environmental stressors may be affected (Carpenter et al., 2006).

Human population growth and economic expansion are widely recognised as major anthropogenic drivers of LULC change (Vitousek, Mooney, Lubchenco, & Melillo, 1997). Approximately one-third to one-half of the Earth's land surface has already been modified considerably by human activities (Vitousek et al., 1997), and the extent of this transformation may increase to compensate for the growing demand for food and natural resources (Bommarco et al., 2013). In response to the concerns about human capability to adapt to a changing environment, interdisciplinary assessments of LULC status and change have become increasingly important subjects of environmental change research (Verburg, Van De Steeg, Veldkamp, & Willemen, 2009).

Since the start of economic reforms in China in 1978, the country has sustained accelerated economic growth and urban expansion. The total population grew from about 980 million people in 1980 to 1.36 billion people in 2013 (National Bureau of Statistics of China, 2014). Resultant social restructuring processes have led to an environmental transformation of unprecedented proportions (Jianguo Liu & Diamond, 2005). To mitigate the adverse impacts, the Chinese government has responded by implementing a series of land reform policies and incentive programs to reduce land degradation and promote sustainable development in rural China (The University of Nottingham. China Policy Institute, 2010).

The Grain for Green Project (GGP), also called the Sloping Land Conversion Program, implemented since 1999, is the largest ecosystem service payment project in the country (Jianguo Liu, Li, Ouyang, Tam, & Chen, 2008; X. Wang, Lu, Fang, & Shen, 2007). The GGP focuses primarily on the reduction of cropland on steep slopes to promote three types of land conversions: cropland to forest, cropland to grassland, and wasteland to forest (The University of Nottingham. China Policy Institute, 2010; Zhou, Zhao, & Zhu, 2012). The project also advocates for prohibition of enclosures for grazing, and sand storm prevention and control (X. Wang et al., 2007). Some of the immediate benefits of the land restoration program include increased forest coverage, control of soil erosion, and reduced spread of wind-blown dust (Fan et al., 2015). However, work is still required to explore the additional ecological, climatic and public health consequences that can result from the long-term implementation of the GGP and other similar environmental initiatives (Jianguo Liu et al., 2008; Roger A. Pielke, 2005). Ningxia Hui Autonomous Region (NHAR) is a province located in arid and semi-arid areas across the Loess Plateau and the Yellow River plains which are priority regions for the implementation of the GGP (Jianguo Liu et al., 2008; The University of Nottingham. China Policy Institute, 2010). The high local poverty rates, the difficult natural environmental conditions and the over-exploitation of natural resources in NHAR have contributed to the deterioration of the local ecological environment in past decades.

Earth observation (EO) data collected using satellite remote sensing and in situ observations, have been extensively used to characterise and monitor LULC change (Broich et al., 2014; Carreiras, Jones, Lucas, & Gabriel, 2014; Hamm, Magalhães, & Clements, 2015; Shalaby & Tateishi, 2007; B. L. Turner et al., 2007; Yuan, Sawaya, Loeffelholz, & Bauer, 2005). Recently, the wide availability of very fine- (<10 m) and fine- (10 to 100 m) resolution imagery from satellite sensors such as Landsat, QuickBird and IKONOS, have provided new opportunities to represent more accurately LULC at finer spatial resolutions (J. Chen et al., 2015; Hamm et al., 2015; Raj, Hamm, & Kant, 2013; Sawaya, Olmanson, Heinert, Brezonik, & Bauer, 2003). EO data and geographic information systems (GIS) have been applied in China to guide scientific activities that focus on the assessment and monitoring of the short- and long-term effects of different land use and management practices implemented at various administrative levels (Fan et al., 2015; Jiyuan Liu et al., 2014; Weng, 2002).

This study aims to quantify and describe the spatial and temporal patterns of climate and land cover change in NHAR and to quantify land cover changes associated with the GGP. Maps that accurately document the local patterns of land cover and climate change in this province can form the basis for future landscape planning and ecosystem management and protection.

This spatially explicit information on environmental change may also help to understand and respond rapidly and effectively to emerging environmental risks for the local population.

## Materials and Methods

### *Study area*

NHAR is a small province located on the upper reaches of the Yellow River in northwest China between latitudes 35°26' N and 39°30' N, and between longitudes 104°50' E and 107°40' E. NHAR shares borders with the Inner Mongolia Autonomous Region in the north, Gansu Province in the south and west and Shaanxi Province in the east. From north to south, the provincial territory stretches 465 km, and from east to west between 45 km and 250 km, with a total area is 66,400 $km^2$. NHAR consists of five prefectures that are subsequently subdivided into counties, townships and villages. By the end of 2014, the total population amounted to 6.6 million people of which 53.6 % were living in urban areas and 46.4% in rural areas (J. Li et al.; Statistical Bureau of Ningxia Hui Autonomous Region, 2014).

NHAR lies at ~1,000 m above sea level. The territory is geographically diverse and consists of three major natural regions that have distinct agricultural production systems: the northern Yellow River Irrigated District (irrigated agricultural system), the central desertified district (a mix of rainfed and irrigated areas with extensive grazing) and the southern mountainous and loess hilly district (with a rainfed agricultural system). These regions cover 23.7%, 45% and 31.3% of the NHAR territory, respectively (J. Li et al.; Y. Li et al., 2013). Elevation increases from north to south with the highest peak at 3,556 meters. In general, the province has a temperate continental monsoon climate and four distinct seasons. Temperature varies from 24℃ in July to –9℃ in January with an annual average of 5°C – 9.9°C. Rainfall varies from 180 to 800 mm per annum increasing from north to south. Most rainfall occurs during the summer and autumn months (80% of the total precipitation in the entire region). The annual average rainfall is 289mm/year. (J. Li et al.).

***Remotely sensed data***

The Landsat Surface Reflectance Climate Data Record (Landsat CDR) was the main source of the data used for land cover classification and change detection analyses. Landsat CDR data sets, also called Landsat level 2A products, are high-level data products that were generated by applying atmospheric correction routines to Landsat Level 1 scenes (Department of the Interior - The United States Geological Survey (USGS), 2016a, 2016b). The Landsat CDR uses the Universal Transverse Mercator (UTM) projection (48N for NHAR). For the study, time series of Landsat CDR data sets processed from Landsat 4-5 Thematic Mapper (Landsat 4-5 TM) and Landsat 8 Operational Land Imager and Thermal Infrared Sensor (Landsat-8 OLI/TIRS) were downloaded for the period 1990 to 2015 at five-year intervals. This time period was selected due to the increased availability of cloud-free data. Images were acquired from the United States Geological Survey (USGS) Earth Explorer website (The United States Geological Survey (USGS)). For most years, four scenes were required to cover the entire NHAR territory. However, due to the presence of clouds in some of the available images from 1995 and 2000, a fifth scene was required to fill the missing data for those years. The primary scene selection criteria were based on acquisition dates. To the extent possible, images were collected from the period June to November each year which corresponds to the summer and autumn growing seasons in NHAR. However, actual image acquisition dates varied depending on the availability of the data. When there were no scenes available for the selected months, the closest-in-time and most cloud-free scenes available were downloaded for the analyses (Table 1).

**Table 1 Specifications for the Landsat scenes used for land cover classification and change detection analyses in Ningxia Hui Autonomous Region from 1990 to 2015**

| Year | Data type | Landsat Scene | Path/Row | Date acquired |
|---|---|---|---|---|
| **1990** | Landsat 4-5 Thematic Mapper | LT51290331989236BJC00 | 129/033 | 24/08/1989 |
| | | LT51290341991242BJC00 | 129/034 | 30/08/1991 |
| | | LT51290351991242BJC00 | 129/035 | 30/08/1991 |
| | | LT51300341993158CLT00 | 130/034 | 07/06/1993 |
| **1995** | Landsat 4-5 Thematic Mapper | LT51290331995253CLT00 | 129/033 | 10/09/1995 |
| | | LT51290341996128CLT00 | 129/034 | 07/05/1996 |
| | | LT51290351996112CLT00 | 129/035 | 21/04/1996 |
| | | LT51300341996215BJC00 | 130/034 | 02/08/1996 |
| | | LT51300341996023CLT00 | 130/034 | 23/01/1996 |
| **2000** | Landsat 4-5 Thematic Mapper | LT51290332000235BJC00 | 129/033 | 22/08/2000 |
| | | LT51290342000235BJC00 | 129/034 | 22/08/2000 |
| | | LT51290352001141BJC00 | 129/035 | 21/05/2001 |
| | | LT51300332000258BJC00 | 130/033 | 14/09/2000 |
| | | LT51300342000242BJC00 | 130/034 | 29/08/2000 |
| **2005** | Landsat 4-5 Thematic Mapper | LT51290332005296BJC00 | 129/033 | 23/10/2005 |
| | | LT51290342005280BJC00 | 129/034 | 07/10/2005 |
| | | LT51290352005280BJC00 | 129/035 | 07/10/2005 |
| | | LT51300342005303BJC00 | 130/034 | 30/10/2005 |
| **2010** | Landsat 4-5 Thematic Mapper | LT51290332010182IKR00 | 129/033 | 01/07/2010 |
| | | LT51290342010198IKR00 | 129/034 | 17/07/2010 |
| | | LT51290352010198IKR00 | 129/035 | 17/07/2010 |
| | | LT51300342010253IKR00 | 130/034 | 10/09/2010 |
| **2015** | Landsat 8 Operational Land Imager and Thermal Infrared Sensor | LC81290332015244LGN00 | 129/033 | 01/09/2015 |
| | | LC81290342015244LGN00 | 129/034 | 01/09/2015 |
| | | LC81290352015196LGN00 | 129/035 | 15/07/2015 |
| | | LC81300342015187LGN00 | 130/034 | 06/07/2015 |

### *Elevation data*

Topographic correction was performed to reduce terrain illumination effects on the retrieved data. To apply the topographic correction algorithm, information on solar position according to the acquisition time of the images, and on the slope and aspect of the terrain are required. Therefore, in addition to the Landsat metadata files, the Advanced Spaceborne Thermal Emission and Reflection Radiometer (ASTER) Global Digital Elevation Model (GDEM) version 2 was downloaded from the USGS Earth Explorer website (The National Aeronautics and Space Administration (NASA) and Ministry of Economy Trade and Industry (METI), 2011; The United States Geological Survey (USGS)). It was necessary to project the ASTER DEM to match the Landsat imagery. Using nearest-neighbour resampling, the GDEM data were projected to the Universal Transverse Mercator (UTM) coordinate system zone 48N and resampled to a 30 m spatial resolution using ArcGIS software version 10.3.1 (Environmental Systems Research Institute (ESRI), 2015).

***Reference data for image classification and validation***

Due to the lack of reference information on land cover information for NHAR during the study period, multiple data sources were required to produce reference data sets for land cover classification (training) and accuracy assessment (validation).

Training data for the years 2000 and 2010 were obtained from random sampling of a combination of relatively fine-scale global maps, the GlobeLand 30 and the global forest/non-forest maps (FNF) (Japan Aerospace Exploration Agency (JAXA); National Geomatics Center of China, 2014). Although GlobeLand 30 was only released in 2014 it has been applied extensively at national and regional levels in various countries with high levels of accuracy (Brovelli, Molinari, Hussein, Chen, & Li, 2015; Jokar Arsanjani, See, & Tayyebi, 2016; Jokar Arsanjani, Tayyebi, & Vaz, 2016; Manakos, Chatzopoulos-Vouzoglanis, Petrou, Filchev, & Apostolakis, 2014; Shi, Nie, Ju, & Yu, 2016; Walker, Stickler, Kellndorfer, Kirsch, & Nepstad, 2010) and evaluation is ongoing. The GlobeLand 30 is a Landsat-based product generated by the National Geomatics Center of China (NGCC) (J. Chen et al., 2015). This product represents the first attempt to create global land cover maps for the years 2000 and 2010 at 30 m resolution (J. Chen et al., 2015). The Japan Aerospace Exploration Agency (JAXA) produced the FNF data sets by classifying 25 m resolution satellite images into forest and non-forest areas. FNF data sets are available for the years 2007, 2008, 2009 and 2010 (Japan Aerospace Exploration Agency (JAXA) & Earth Observation Research Center (EORC)).

The ArcGIS software (Environmental Systems Research Institute (ESRI), 2015) was used to generate random samples of training points from the GlobeLand 30 and FNF data sets for the years 2000 and 2010. A total of approximately 500 training sites were selected for each year. In this way, it was possible to ensure that all land cover categories were adequately represented in the training statistics. Training data for these two years were not limited to the global land cover and FNF products. All the selected training points were cross-checked against historical imagery from Google Earth Pro (GEP) version 7.1.5.1557 (Google Inc., 2015). Google Earth archives display different forms of imagery obtained from multiple sources such as Landsat and QuickBird satellite sensors and various providers of digital photographs (Lemmens, 2011). GEP software is a widely-used platform for the collection of high resolution geo-referenced information on land cover, and also for the validation of land cover classification maps (Cha & Park, 2007; Chen, Marter-Kenyon, López-Carr, & Liang, 2015; Q. Hu et al., 2013; Lu, Hernandez, & Ramsey, 2015). GEP images from 2001, which is the earliest time point from which data are available for NHAR, and 2010 were used to evaluate the reference data. Training points that were located in indistinct areas in the GEP imagery or in areas that were covered by clouds were removed from the reference data sets.

The training data for 2000 and 2010 were also checked against GEP historical images from 2005 and 2015, respectively. Both, data sets and images were used to determine visually if land cover had changed between the periods 2000–2005 and 2010–2015. Training points from land areas that changed were discarded to locate and define training signatures for 2005 and 2015.

There were no historical records available for NHAR for the years 1990 and 1995 in GEP. Therefore, training data points for these years were derived from the reference data collected for 2000. Training sites from areas that were likely to remain unchanged based on previous visual interpretation of the GEP historical imagery were selected. In addition, the 1 km spatial resolution land use maps of China produced and provided by the Chinese Academy of Sciences for the 1980s, 1995 and 2000 served as supplementary information to define land cover features in the region.

For all images, visual interpretation of the Landsat data was also implemented to improve ground truth estimation. Visual comparisons of multiple sets of three spectral band combinations were conducted using ENVI software version 5.3 (Exelis Visual Information Solutions, 2015). This approach was used to better distinguish the different categories of the land cover scheme.

Reference validation data sets for accuracy assessment were created by collecting space- and time-referenced data uploaded to the website Panoramio (Google Inc.). The website is a photo-sharing service that contains geo-tagged photos from around the world. Web-based photo-sharing platforms, like Panoramio, are becoming an important data source with potential applications in multiple research contexts (Dong et al., 2014; Yu et al., 2014; Zhou et al., 2012).

Sets of photos for each year were downloaded and labelled manually based on visual interpretation and using the GlobeLand30 land cover classification scheme. Data were imported into ArcGIS to be projected to the same UTM zone used for the satellite images (Environmental Systems Research Institute (ESRI), 2015). Reference points were buffered by 15 m to generate the training site polygons that were used to assess classification accuracy. Although most polygons were effective in distinguishing among different land cover types, the use of this type of data may introduce a level of uncertainty into the analyses (Fonte, Bastin, See, Foody, & Lupia, 2015). Therefore, all polygons of each validation class were checked against historical satellite imagery from GEP. Reference data located in areas where land cover type was questionable were excluded from the analyses. All reference data sets used for accuracy assessments included at least 50 polygons with approximately 2-3 pixels each.

### ***Climate data***

Monthly mean temperature and precipitation data records for the period January 1 1980 to December 31 2013 were analysed. Data were at first collected from 16 local weather stations and interpolated by the Chinese Academy of Sciences using the Inverse Distance Weighting (IDW) method.

The Chinese Academy of Sciences provided the monthly averages of the climate data in a raster format at the spatial resolution of 1 km. An administrative boundary map of the province was downloaded from the DIVA-GIS website (DIVA GIS). The climate data sets were imported into ArcGIS and linked spatially to the boundary map (Environmental Systems Research Institute (ESRI), 2015). Monthly records were summed in the GIS to provide annual, summer (June, July and August) and winter (December, January and

February) weighted mean series. The weights were the number of days in a month. Temperature and precipitation anomalies were also calculated for each pixel and year to define parameters in subsequent statistical models. An anomaly is defined as the deviation of a variable of interest at a given location and a particular time from the long-term average for that location. The reference period used in the study to calculate temperature and precipitation anomalies was January 1 1980 to December 31 2013. A positive anomaly indicates that the parameter under study was higher than the baseline, while a negative value indicates that the parameter was lower than the baseline. This anomaly-based approach was used to improve the consistency of the climate data for subsequent analyses (Jones, New, Parker, Martin, & Rigor, 1999).

Because the trend analyses used pixel-based models, a selection of a random sample of 700 locations from each data set (53,157 pixels) was required to optimise the statistical methods.

***Image classification***

Pre-processing of the Landsat data was performed using the Landsat package (version 1.08) (Goslee, 2011) in the RStudio software Version 0.98.1091 (RStudio Team, 2014). The Minnaert topographic correction method was applied independently to each spectral band to improve image comparability between dates. The spectral bands were stacked together and saved as a multiband image in TIFF format. To reduce the effects of clouds, cloud and cloud shadow removal were performed. The Landsat scenes for each date were mosaicked together and classified using ENVI version 5.3 (Exelis Visual Information Solutions, 2015). The maximum likelihood algorithm was the selected method for the process of supervised classification. Assuming a normal distribution of the data, this algorithm considers both the variance and covariance of class signatures to assign unknown pixels to a specific land cover class (Strahler, 1980).

The land cover classes were grouped into seven categories according to the spectral reflectance values and the objectives of the study. Because the reference data for classification was derived primarily from GlobeLand30, the classification scheme adopted was based on the land cover classification system established by the NGCC (Table 2).

**Table 2 Land cover classification scheme and definitions**

| Code | Land cover type | Description | Content |
|---|---|---|---|
| 1 | Water bodies | All areas of water | Streams and canals, lakes, reservoirs, bays and estuaries |
| 2 | Artificial surfaces | Land modified by human activities | Residential areas, industrial and commercial complexes, transport infrastructure, communications and utilities, mixed urban or built-up land and other built-up land |
| 3 | Bare or sparsely vegetated areas | Areas with little or no "green" vegetation present | Dry salt flats, sandy areas, bared exposed rock and mixed barren land |
| 4 | Herbaceous vegetation | Areas characterized by natural or semi-natural vegetation | Grasses and forbs |
| 5 | Cultivated land | Areas where the natural vegetation has been removed/modified and replaced by other types of vegetative cover that have been planted for specific purposes such as food, feed and gardening | Cropland and pasture, orchards, groves, vineyards, nurseries and ornamental horticultural, other cultivated land |
| 6 | Shrubland | Natural or semi-natural woody vegetation with aerial stems less than 6 meters tall | Evergreen and deciduous species of true shrubs and trees or shrubs that are small or stunted |
| 7 | Forest | Areas characterized by tree cover or semi-natural woody vegetation greater than 6 meters tall | Deciduous forest, evergreen forest and mixed forest |

Post-classification refinements were applied to reduce errors in the process of classification. Due to significant spectral confusion among the classes, artificial surfaces and bare or sparsely vegetated areas, these two classes were merged and represented as a single category in the maps and subsequent analyses.

Using ENVI software, confusion matrices were calculated to assess the accuracy of the land cover classification maps. A confusion matrix is a simple cross-tabulation of each mapped class vs. the reference information (Foody, 2002; Lillesand, Kiefer, & Chipman, 2014). The overall accuracy of the classification, Kappa coefficient and user's and producer's accuracy were derived from the confusion matrices. The Kappa statistic reflects the difference between actual agreement between reference data and the classified maps and the agreement expected by chance. A kappa value of 1 indicates perfect agreement, while a value of 0 indicates no agreement (Foody, 2002). User’s accuracy provides an estimate of the probability that a pixel from the land cover map matches the same category in the reference data (it measures errors of commission), whereas the producer’s accuracy estimates the probability that a reference pixel has been mapped correctly (it measures errors of omission) (Foody, 2002; Lillesand et al., 2014).

***Land cover change detection analysis***

A post-classification change detection technique was performed using ENVI software (Exelis Visual Information Solutions, 2015). Cross-tabulation analyses were conducted to identify changes in land cover between 6 different time intervals 1990–1995, 1995–2000, 2000–2005, 2005–2010, 2010–2015 and 1990–2015. These tables indicate the number of pixels of a given class at time $t_1$ that are classified as the same or different class at time $t_2$

(from – to). This supports identification of changes in land cover as well as the identification of areas that have not changed.

***Climate trend analysis***

Precipitation and temperature trend analyses at annual and seasonal (summer/winter) temporal resolution were carried out by applying a linear model in a Bayesian geostatistical framework. Six separate geostatistical models (annual, summer and winter for temperature and precipitation) were developed using the OpenBUGS software, version 3.2.3 (MRC Biostatistics Unit, 2014). Each of these models incorporated a parameter for the anomaly of the climate variable and a term to model the mean trend for the province.

Each model assumed that the annual and seasonal averages of temperature/precipitation measurements, $Y$, for the $i$th location, ($i$ = 1. . .700) in the $j$th year (1980‑2013) followed a normal distribution with mean ($\mu_{ij}$) and variance $\sigma_t^2$, that is,

$$Y_{ij} \sim Normal(\mu_{ij}, \sigma_t{}^2)$$

$$\mu_{ij} = \alpha + \beta_i \times T_j + \lambda_j \times T_j$$

where $\alpha$ is the intercept, $\beta_i$ (the main parameters of interest), modelled as a spatially-smoothed random effect, are the magnitudes of the trends for each location, $T$ is the number of years from the baseline year (1980), and $\lambda$ is the mean trend for the province. The spatial correlation in $\beta_i$ was assumed to be an exponential function of the distance between points, i.e. $\sigma_2{}^2\exp(-\rho d_{kl})$, where $d_{kl}$ is the straight-line distance between pixels $k$ and $l$, $\sigma_2{}^2$ is the geographical variability known as sill and $\rho$ is a smoothing parameter that controls the rate of correlation decay with distance.

A normal prior distribution was specified for $\alpha$ and $\lambda$ (with a mean=0 and a precision=0.001). The priors for the precision parameters ($1/\sigma_t^2$) were specified using non-informative gamma distributions with shape and scale parameters equal to 1. The prior distribution of phi (rate of decay) was uniform with upper and lower bounds set at 0.01 and 100.

A burn-in of 1000 iterations was run and discarded. Subsequent blocks of 10,000 iterations were run and examined for convergence. Visual inspection of the posterior density and history plots was used to assess convergence which occurred at approximately 20,000 iterations for each model. After convergence, ten thousand iterations were run and the values from the posterior distributions of each model parameters were stored for the analysis. The posterior mean and 95% credible intervals of the posterior distributions were used to summarise the parameters.

ArcGIS (Environmental Systems Research Institute (ESRI), 2015) was used to interpolate and generate maps that represent the spatial distribution of the relative trend in annual, summer and winter temperature and precipitation anomalies in NHAR for the period January 1980–December 2013. These maps were created by calculating the relative posterior means of the trend from the provincial average and interpolating the values using the inverse distance interpolation technique. Thus, maps produced showed areas where the trend was higher or lower than the overall average.

## Results

### *Land cover classification and change detection analysis*

Confusion matrices showed that the overall classification accuracies were higher or equal to 80% and the total Kappa coefficients were greater than 0.7. These results represent a substantial agreement between the reference data sets and the classified maps (Landis & Koch, 1977). The Kappa coefficients for 1990, 1995, 2000, 2005, 2010 and 2015 were 0.83, 0.83, 0.78, 0.72, 0.74 and 0.80, respectively. Most user's and producer's accuracies of individual classes were also generally high, ranging from 60% to 100%.

Single date land cover maps were produced for each study year to show the spatial distribution of six land cover types in NHAR (Fig 1.). The geospatial extent for each individual class for all data products and the change statistics for 1990 and 2015, which were the temporal extremes of the project were calculated (Table 3).

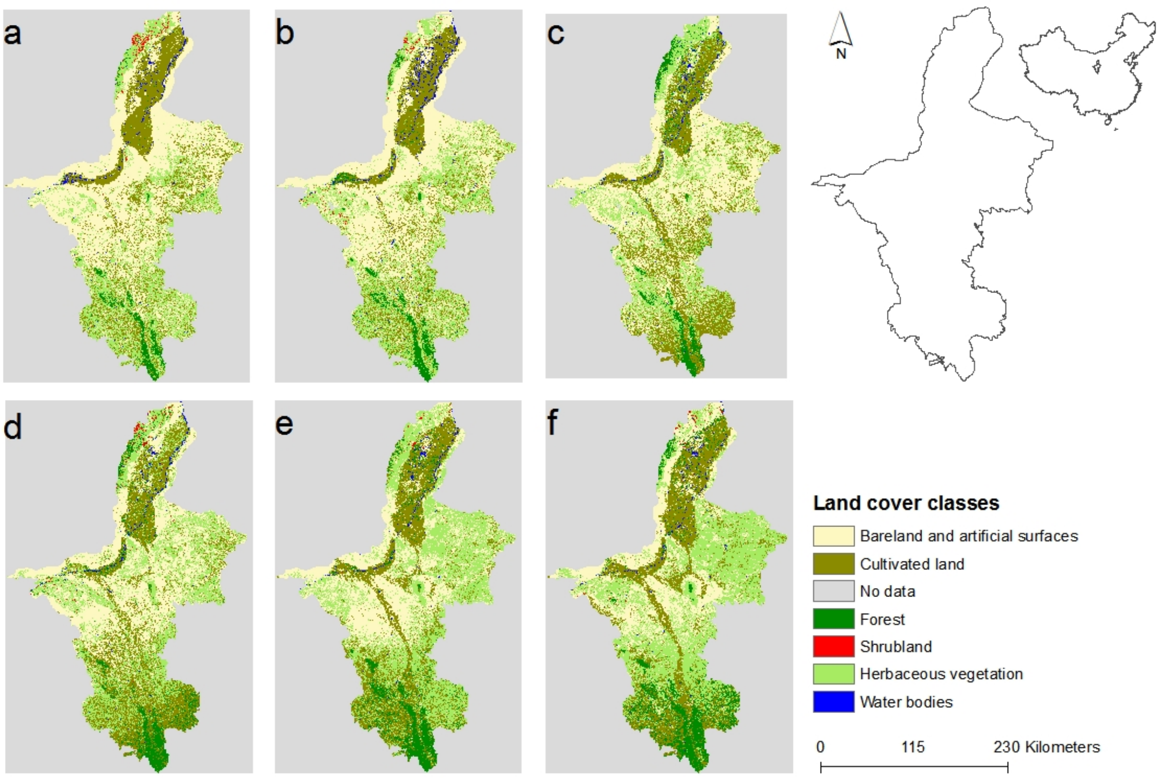


**Fig. 1 Land cover classification maps for NHAR from (a) 1990, (b) 1995, (c) 2000, (d) 2005, (e) 2010, (f) 2015 and map of the location of the province in China.**

From 1990 to 2015, herbaceous vegetation, cultivated land and forest increased by approximately 708,600 ha (12.2% of the study area), 164,300 ha (2.9%) and 410,200 ha (7.1%), respectively. Shrubland decreased by 22,000 ha (0.4%) and water decreased by 10,300 ha (0.2%). The largest relative change for the period 1990-2015 was observed in the area covered by forest, which increased by 273.1%. Forest expanded consistently in all periods, with the greatest increase occurring between 2010 and 2015. The change in forest was followed by the increase in herbaceous vegetation, 49.8%, and in cultivated land, 12.3%. Shrubland and water decreased, respectively, 66.7% and 22.2%. Although the extent of water and shrubland may have changed from year to year due to annual variability in precipitation and temperature, the minor changes observed in this category are likely to be partially explained by classification errors. Because artificial surfaces and bareland were merged into one a single class, it is difficult to interpret the changes observed in this land cover category over time.

**Table 3 Summary statistics of land cover maps from Ningxia Hui Autonomous Region by area (000 hectares)**

| Land cover class | 1990 | 1995 | 2000 | 2005 | 2010 | 2015 | Relative change 1990-2015 (%) |
|---|---|---|---|---|---|---|---|
| | Area (%) | Area (%) | Area (%) | Area (%) | Area (%) | Area (%) | |
| Water bodies | 53.1 (0.9) | 84.6 (1.5) | 59.3 (1) | 47.9 (0.8) | 43.6 (0.8) | 42.8 (0.7) | -22.2 |
| Herbaceous vegetation | 1,409.2 (24.5) | 1,543.2 (26.8) | 1,455.7 (25.2) | 1,687.7 (29.3) | 2,022.3 (35.1) | 2,117.8 (36.7) | 49.8 |
| Cultivated land | 1,356.1 (23.5) | 1,257.7 (21.9) | 1,628.8 (28.3) | 1,543.3 (26.8) | 1,504.4 (26.1) | 1,520.4 (26.4) | 12.3 |
| Shrubland | 35.4 (0.6) | 27.0 (0.5) | 0.27 (0.004) | 33.9 (0.6) | 7.8 (0.1) | 13.4 (0.2) | -66.7 |
| Forest | 147.6 (2.6) | 227.8 (4) | 290.4 (5.1) | 380.4 (6.6) | 455.1 (7.9) | 557.8 (9.7) | 273.1 |
| Bareland and artificial surfaces | 2,757.9 (47.8) | 2,611.7 (45.4) | 2,321.9 (40.3) | 2,066.1 (35.9) | 1,726.1 (30) | 1,507.1 (26.2) | -45.2 |

To further evaluate the results of land cover conversions, matrices of land cover changes from 1990 to 1995, 1995 to 2000, 2005 to 2010, and 2010 to 2015 were created (Table 4).

**Table 4 Matrices of land cover changes (000 hectares) from 1990 to 2015**

**a. Period 1990-1995**

| 1995 | **1990** | | | | | | 1995 Total |
|---|---|---|---|---|---|---|---|
| | Water bodies | Herbaceous vegetation | Cultivated land | Shrubland | Forest | Bareland and artificial surfaces | |
| Water bodies | 40 | 3.1 | 33.8 | 0.3 | 0.1 | 7 | 84.3 |
| Herbaceous vegetation | 0.8 | 1,104.5 | 211.6 | 17.5 | 10.8 | 198 | 1,542 |
| Cultivated land | 6.7 | 92.5 | 1,024.5 | 0.6 | 5.1 | 128.2 | 1,257.6 |
| Shrubland | 0.2 | 10.5 | 0.4 | 10.1 | 0.003 | 5.7 | 27 |
| Forest | 3.8 | 54.1 | 35.8 | 1.7 | 131 | 0.6 | 227 |
| Bareland and artificial surfaces | 0.8 | 142.7 | 49.9 | 5.1 | 0.1 | 2,411.9 | 2,610.5 |
| Difference | 32 | 134.6 | -98.4 | -8.4 | 80 | -140.90 | |
| 1990 total | 52.3 | 1,407.4 | 1,356 | 35.4 | 147 | 2,751.4 | 5,748 |

**b. Period 1995-2000**

| 2000 | 1995 | | | | | | 2000 Total |
|---|---|---|---|---|---|---|---|
| | Water bodies | Herbaceous vegetation | Cultivated land | Shrubland | Forest | Bareland and artificial surfaces | |
| Water bodies | 33.6 | 2.4 | 15.2 | 0.4 | 1.7 | 5.8 | 59.3 |
| Herbaceous vegetation | 18.6 | 634.7 | 226.9 | 15.5 | 44.4 | 513.1 | 1,453.1 |
| Cultivated land | 21.1 | 387.3 | 685.5 | 0.2 | 43.6 | 490.75 | 1,628.4 |
| Shrubland | 0 | 0.1 | 0.003 | 0.1 | 0.01 | 0.1 | 0.3 |
| Forest | 3.7 | 59.8 | 77.1 | 5.3 | 133.6 | 10.9 | 290.3 |
| Bareland and artificial surfaces | 7.5 | 457.8 | 252.8 | 5.5 | 3.7 | 1589.7 | 2,317.1 |
| Difference | -25.2 | -88.9 | 370.8 | -26.7 | 63.3 | -293.3 | |
| 1995 total | 84.5 | 1,542 | 1,257.6 | 27 | 227 | 2,610.4 | 5,748 |

**c. Period 2000-2005**

| 2005 | 2000 | | | | | | 2005 Total |
|---|---|---|---|---|---|---|---|
| | Water bodies | Herbaceous vegetation | Cultivated land | Shrubland | Forest | Bareland and artificial surfaces | |
| Water bodies | 27.5 | 8.1 | 5.7 | 0 | 2.2 | 4 | 47.5 |
| Herbaceous vegetation | 10.3 | 687.5 | 373.8 | 0.1 | 47.7 | 566 | 1,685.4 |
| Cultivated land | 7.8 | 326.1 | 786.9 | 0.005 | 83.3 | 338 | 1,542.1 |

| | | | | | | | |
|---|---|---|---|---|---|---|---|
| Shrubland | 1 | 17.9 | 1.7 | 0.1 | 9.9 | 3.2 | 33.8 |
| Forest | 5.8 | 82.8 | 133.3 | 0.04 | 139.6 | 17.5 | 379 |
| Bareland and artificial surfaces | 6.9 | 330 | 327 | 0 | 7.5 | 1,389 | 2,060.4 |
| Difference | -11.8 | 233 | -88.3 | 33.6 | 88.8 | -257.3 | |
| 2000 total | 59.3 | 1,452.4 | 1,628.4 | 0.2 | 290.2 | 2,317.7 | 5,748 |

**d. Period 2005-2010**

| 2010 | 2005 Total | | | | | | 2010 Total |
|---|---|---|---|---|---|---|---|
| | Water bodies | Herbaceous vegetation | Cultivated land | Shrubland | Forest | Bareland and artificial surfaces | |
| Water bodies | 25.5 | 5.3 | 5.4 | 0.1 | 1.7 | 5.5 | 43.5 |
| Herbaceous vegetation | 2.07 | 922 | 460.8 | 21.8 | 72.9 | 542.7 | 2,022.3 |
| Cultivated land | 9.9 | 386.1 | 753.8 | 2.1 | 95.5 | 257.2 | 1,504.6 |
| Shrubland | 0.2 | 1.4 | 0.2 | 3.4 | 0.7 | 1.84 | 7.7 |
| Forest | 3.8 | 82.2 | 168.3 | 1 | 193 | 6.8 | 455.1 |
| Bareland and artificial surfaces | 6 | 289 | 154 | 5.5 | 15 | 1245 | 1,714.5 |
| Difference | -4 | 1,100.3 | -37.9 | -26.2 | 76.1 | -345.5 | |
| 2005 total | 47.5 | 1,686 | 1,542.5 | 33.9 | 379 | 2,060 | 5,748 |

**e. Period 2010-2015**

| 2015 Total | 2010 Total | | | | | | 2015 Total |
|---|---|---|---|---|---|---|---|
| | Water bodies | Herbaceous vegetation | Cultivated land | Shrubland | Forest | Bareland and artificial surfaces | |
| Water bodies | 26.8 | 1.4 | 5.6 | 0.3 | 3.1 | 5.5 | 42.8 |
| Herbaceous vegetation | 1 | 1,294.22 | 276.6 | 0.4 | 45.7 | 500 | 2,117.2 |
| Cultivated land | 10.8 | 235.5 | 963.9 | 0.2 | 129.5 | 180 | 1,519 |
| Shrubland | 0.03 | 6.7 | 0.3 | 2.8 | 0.3 | 3.3 | 13.4 |
| Forest | 0.8 | 123.9 | 152.4 | 1.2 | 271 | 8.4 | 557.7 |
| Bareland and artificial surfaces | 3.9 | 360.5 | 105.5 | 2.9 | 5.6 | 1,017.5 | 1,496 |
| Difference | -0.6 | 95.2 | 15 | 5.6 | 102.5 | -218.7 | |
| 2010 total | 43.4 | 2,022 | 1,504.3 | 7.8 | 455.2 | 1,714.7 | 5,748 |

**f. Period 1990-2015**

| 2015 Total | 1990 | | | | | | 2015 Total |
|---|---|---|---|---|---|---|---|
| | Water bodies | Herbaceous vegetation | Cultivated land | Shrubland | Forest | Bareland and artificial surfaces | |
| Water bodies | 15.9 | 2.9 | 14.7 | 0.1 | 0.3 | 8.9 | 42.8 |
| Herbaceous vegetation | 2.4 | 689.4 | 307 | 12.5 | 9.9 | 1,096 | 2,117.2 |
| Cultivated land | 27.5 | 279.9 | 724.6 | 1.7 | 16.1 | 470 | 1,519.8 |
| Shrubland | 0.1 | 5.2 | 0.6 | 2.4 | 0.01 | 5.1 | 13.4 |
| Forest | 2.8 | 230.5 | 142.5 | 1.9 | 120.7 | 59.3 | 557.7 |
| Bareland and | 3.4 | 199 | 166.7 | 16.7 | 0.6 | 1110.4 | 1,496.8 |

| | | | | | | | |
|---|---|---|---|---|---|---|---|
| artificial surfaces | | | | | | | |
| Difference | -9.3 | 710.2 | 163.70 | -22 | 410.1 | -1,253.2 | |
| 1990 total | 52.1 | 1,407 | 1,356.1 | 35.4 | 147.6 | 2,750 | 5,748 |

The results suggest that the area covered by herbaceous vegetation increased in all periods except in the interval 1995-2000 when it decreased by 88,900 ha. Although cultivated land increased over the whole study period, it experienced a decrease in the first five years of the study and between 2000 and 2010.

In 2000, prior to the implementation of the GGP, forest, herbaceous vegetation and cultivated land covered an area of approximately 290,433 ha, 1,455,755 ha and 1,628,894 ha, respectively. By 2015, forest and herbaceous vegetation extended to 557,807 ha and 2,117,812 ha, while cultivated land was reduced to 1,520,435 ha.

The increase in forest resulted mainly from conversion of cultivated land and herbaceous vegetation in the twenty-five-year period. Of the 410,200 ha of total growth in forest between 1990 and 2015, 53.8% was converted from herbaceous vegetation and 30.8% from cultivated land. Although it is not possible to estimate the amount of land conversion, the increase in herbaceous vegetation, presumably mostly came from bareland.

The changes in land cover that occurred in NHAR between 1990 and 2015 were not spatially homogeneous. The six land cover maps produced in the study reveal that land cover changes varied among the three different geographical regions. In general, the central desertified district and the southern mountainous and loess hilly district were the most transformed. Forest growth primarily occurred in the north and south of the province, in areas of the Helan and Liupan mountains in the north and south, respectively. The increase in herbaceous vegetation was mainly distributed in the central arid area of the province, and around the margin of forestland. Cultivated land dominated the landscape on the big plains of the northern Yellow River Irrigated District with a progressive linear expansion in the central area.

***Temperature and precipitation trends***

Maps of the spatial distribution of annual, summer and winter temperature and precipitation anomaly trends were created (Fig. 2). The overall results found statistically significant positive trends in annual, summer and winter temperatures in most of NHAR for the period January 1980–December 2013. These temporal trends were spatially variable across the province. Annual temperature trends were significantly higher in the north-west of the province and the western part of the central desertified district, and significantly lower in the south. The spatial pattern of annual warming was similar for summer temperature trends but with higher magnitudes. The greatest trend magnitude in temperature anomalies appeared in winter, with an increase of 2.9 °C/decade. The spatial distribution of the winter trend varied slightly from the spatial pattern described for annual and summer temperatures. In winter, temperature rose rapidly in areas located throughout the central part of the province. Similar to annual and summer temperatures, a significantly lower trend was also found in winter in the southern mountainous area.

The analysis of the time series of annual precipitation anomalies revealed that there was a slight positive trend in annual precipitation for NHAR for the period January 1980‑December 2013 (Fig 2d). In general, there was a small magnitude change in annual precipitation, 0.11 mm/decade for the whole period with distinctive spatial and seasonal patterns. A statistically significant upward trend was observed in the northern and central part of the province, whereas significant negative trends were found in the south. The annual precipitation trend magnitude varied between -7 mm and 7 mm per decade from the provincial average trend.

The summer precipitation anomaly for the whole province showed a statistically significant decreasing trend. The spatial pattern of the trend was similar to that of annual precipitation (Fig. 2e). Significant positive trends were mostly found in the north and centre of NHAR and significantly negative trends were observed in the south. The range of trend magnitude in summer precipitation varied between -25 mm and 30 mm per decade from the provincial average trend.

The highest increasing precipitation trend for the entire province was observed in the winter season, with an increase of 2.4 mm over the study period. However, winter precipitation anomaly trends exhibited an opposite spatial distribution when compared to that of annual and summer precipitation. Winter precipitation showed negative trends in the northern and central part of NHAR and positive trends in the southern mountainous and loess hilly district (Fig. 2e). The magnitude of this trend varied between -2 mm and 5 mm per decade from the provincial average trend.

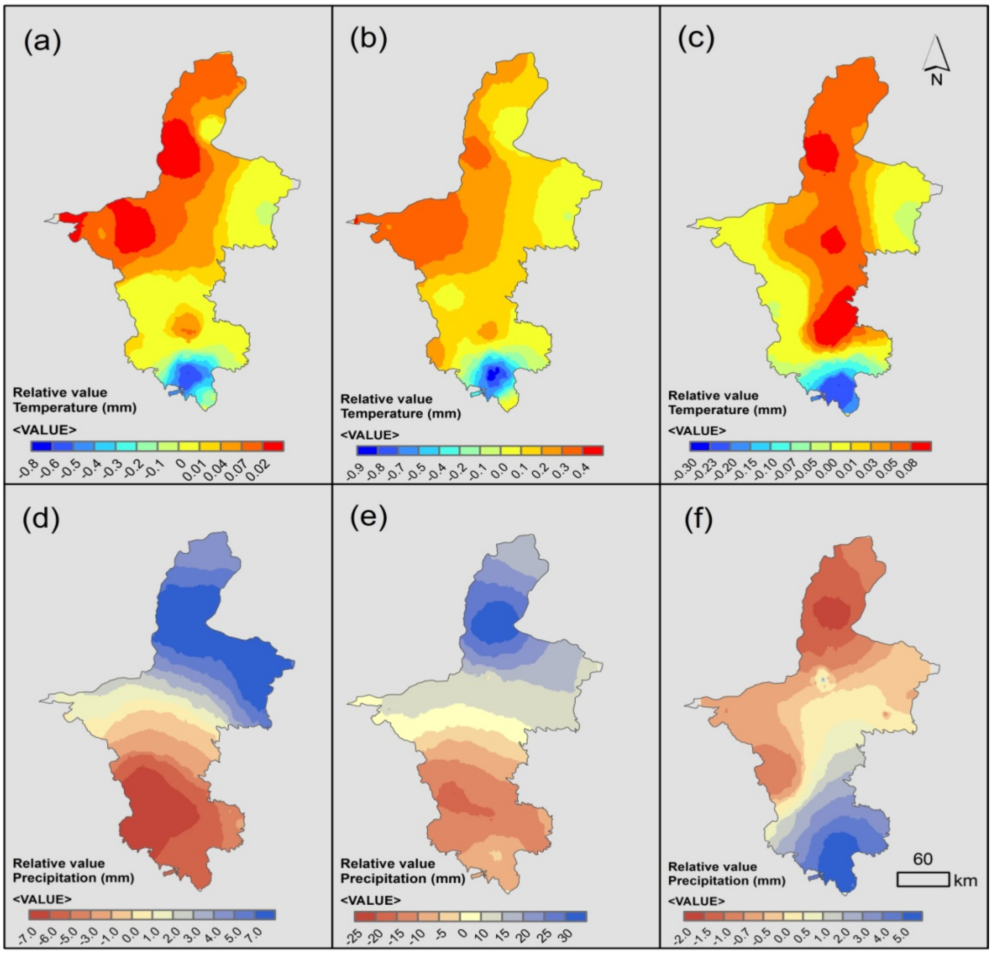


**Fig. 2 Maps of the spatial distribution of (a) annual, (b) summer and (c) winter temperature trends, and (d) annual, (e) summer and (f) winter precipitation trends in NHAR for the period 1 January 1980 to 31 December 2013. Note, the values presented in the figure are relative to the provincial average per decade.**

## Discussion

The results of the present study are consistent with previous environmental assessments conducted in western China to describe the land cover changes that have occurred in regions where ecological restoration policies were adopted (S. Cao, Chen, & Yu, 2009; Fan et al., 2015; Zhao, Lv, & Dai, 2010). According to national estimates, by 2006, the GGP policy was responsible for the conversion of almost 9 million ha of cultivated land into forest and herbaceous vegetation, and the afforestation of 11.7 million ha of barren land (Jianguo Liu et al., 2008). In the Loess Plateau, a region commonly characterised by drought, desertification and soil erosion, a rapid increase in vegetation cover was reported in the early 2000s after the implementation of the pilot phase of the programme (Fan et al., 2015; Xin, Xu, & Zheng, 2008). The land cover changes observed in NHAR are in agreement with the key environmental goals of the GGP and previous short-term (ten years or less) land cover assessments conducted in the province using remote sensing or official national reports (J. Li et al.; Qi, Wang, & Wang, 2003; Y. Wang, Gao, Wang, & Qiu, 2014; Zhang, Tu, & Mol, 2008). In this study, forest, herbaceous vegetation and cultivated land coverages increased between 1990 and 2015. Similar findings were reported in other provinces such as Shaanxi located at the middle reaches of the Yellow River Basin (H. Chen et al., 2015), and Sichuan Province, located at the upper reaches of the Yangtze River (Yan-qiong, Guo-jie, & Hong, 2003).

Climate in NHAR follows the same long-term warming and drying trend described for China (L. Cao, Zhu, Tang, Yuan, & Yan, 2016). From January 1980 – December 2013 the trend in annual, summer and winter temperatures showed a significant increase. More rapid warming was observed during the winter season. Average temperature trends decreased with altitude. The more rapid increase in temperature was observed in areas located in the north and central part of the province and a slower warming trend was observed in areas near the Liupan Mountains in the south. Similar statistically significant positive temperature trends for NHAR have been reported by other authors (J. Li et al.; Y. Li et al., 2013). Contrasting with previous studies that reported a downward trend in annual precipitation, we noted a slight increase in the averaged annual precipitation trends for NHAR.  Winter precipitation increased and summer precipitation decreased following the same trend as other local reports (Y. Li et al., 2013).

The spatial variation in the distribution of the six land cover types and changes in NHAR between 1990 and 2015 can be explained partially by the contrasting climatic and topographic characteristics of the three geographical regions of the province. However, there are also other local environmental and socio-economic factors that may influence the local land use practices and lead to land cover change. NHAR is vulnerable to numerous meteorological hazards that have the potential to damage the land surface (Y. Li et al., 2013). Drought, floods, torrential rain and high and low temperature stresses are particularly frequent in the region (Y. Li et al., 2013). Between 2004 and 2006, a severe drought affected the region causing an important reduction in the availability of water for industrial and agricultural purposes (Y. Li et al., 2013; Yang et al., 2015). This meteorological event had important environmental and economic consequences for the province, some of which were evident in this study. Decreases of 126,200 ha of cultivated land and 15,800 ha of water were observed between 2000 and 2010, particularly in the northern and the central part of the province, where irrigation water is mainly diverted from the Yellow River. These findings are in agreement with those mentioned previously in a report that promotes better adaptation strategies to minimise the effects of future environmental hazards (Yang et al., 2015).

NHAR is currently undergoing economic transition processes that also affect the use of land directly and indirectly (C. Wang, Yang, & Zhang, 2011). Land conversion is linked directly to socioeconomic development due to the effects of economic growth on urban expansion and exploitation of natural resources (C. Wang et al., 2011). Economic growth also influences positively the spatial structure of land use patterns by improving income opportunities from non-agricultural sectors, causing income diversification and promoting rural-urban migration (Peng, 2011). While current evidence recognises the role of national ecological rehabilitation projects in China, there is still a need for more holistic and rational approaches that examine the contributions of other economic and social factors in the process of landscape restoration in the country.

Ecological restoration policies, if implemented appropriately, can be effective measures to address pressing environmental concerns. However, the mixture of natural and artificially modified landscapes has also important implications for the structure and function of ecosystems and human health. Environmental change has the potential to compromise food security by influencing food availability, accessibility, utilization and systems stability (Ingram, Ericksen, & Liverman, 2012). In addition, alterations to the climate and landscape features have been increasingly associated with variations in human disease patterns. This is particularly important for infectious diseases, where environmental change impacts on the geographic range of various mosquito-borne diseases such as malaria, dengue and leishmaniasis (Caminade et al., 2014; Colón-González, Fezzi, Lake, & Hunter, 2013; González, Paz, & Ferro, 2014) and non-mosquito-borne helminth infections, such as schistosomiasis and echinococcosis (Giraudoux et al., 2013; Y. Hu et al., 2013). In hyper-endemic areas for echinococcosis in western China the geographical patterns of alveolar echinococcosis infection have been associated with the recent implementation of land reform policies in the region (Giraudoux et al., 2013; Pleydell et al., 2008). Land cover transformations that result from land reforms are likely to alter the transmission of *Echinococcus spp.* by influencing human behaviour, animal population dynamics, spatial and temporal overlap of intermediate and definitive hosts and the survival of the parasite eggs in the external environment (Cadavid et al., 2015).

Although some effects of global environmental change can be anticipated, most of the impacts depend on local vulnerabilities and the implementation of effective strategies for adaptation. Accurate predictions of LULC and climate change can only be estimated when there is an adequate availability of local socio-economic and baseline data. This study allowed us to identify spatial and temporal patterns in climate and land cover change trends in NHAR in the last 30 years. The findings provide accurate information, in space and time, and visual representations of the areas that are most affected by climate and land cover change. Therefore, these results are a reasonable starting point from which to conduct future research in NHAR to explore, monitor and predict future environmental change and its short- and long-term effects on the well-being of the population.

The main challenges of the study include the limited availability of historical satellite and reference data to train the classifier and validate the land cover maps. When analysing time-series data sets, quality and consistency in the data are essential to identify the real changes that occur in the environment. In this study, part of the disagreement between the Landsat scenes and the reference training data sets may be attributed to the fact that there were no images for the specified period in some locations. For some years it was necessary to derive data from different growing seasons. In addition, the use of Globeland 30 and the FNF maps may have introduced some uncertainty into the analysis because they are also land cover products that may contain classification errors that by default were included in the analyses. Although the reference training data obtained from these maps allowed us to classify the satellite images with good accuracy, a more traditional approach that incorporates different data sources and a combination of field studies is the recommended approach. The use of interpolated surfaces for the estimation of the climate trends also represented a challenge for the interpretation of the results. The interpolated surfaces were based on only 16 meteorological stations and the precision of the interpolated values at individual point locations may vary considerably over the entire study area. This is a particularly important point for the interpretation of the trends in those areas where the distribution of meteorological stations is sparse. We believe that a meaningful analysis on climate change can only be achieved with the utilization of consistent and long-term climate records, and networks that are sufficiently dense to capture significant spatial variability. The land cover classification scheme used in the study was derived from the land cover classification system established by the NGCC. Although the use of this legend allowed comparability between land cover datasets, the interpretation of the land cover changes found in the study with respect to the GGP goals also represented a challenge. Based on similarities of definitions, the changes found in herbaceous vegetation and cultivated land were compared to the project goals with respect to grasslands and croplands, respectively.

The results of the analysis of land cover change conducted in this study concur with the large-scale impact of the GGP in increasing forest and herbaceous vegetation coverages and in regenerating bareland areas. These changes occurred within the context of climate warming and changing precipitation patterns. The southern mountainous areas of NHAR became more forested, warmer at a slower rate than the rest of the province, and wetter in the winter months.

**Acknowledgements**

The authors are grateful to the Chinese Academy of Sciences for providing us with the climate data from 1980 to 2013. We acknowledge financial support by the National Health and Medical Research Council (NHMRC) of Australia of a NHMRC Project Grant (APP1009539). AMCR is a PhD Candidate supported by a Postgraduate Award from The Australian National University; ACAC is a NHMRC Senior Research Fellow; DPM is a NHMRC Senior Principal Research Fellow; and DJG is a NHMRC Career Development

Fellow. The funders had no role in study design, data collection and analysis, decision to publish, or preparation of the manuscript.

## References


Blaikie, P., & Brookfield, H. (2015). *Land degradation and society*: Routledge.

Bommarco, R., Kleijn, D., & Potts, S. G. (2013). Ecological intensification: harnessing ecosystem services for food security. *Trends in ecology & evolution, 28*(4), 230-238.

Broich, M., Huete, A., Tulbure, M., Ma, X., Xin, Q., Paget, M., . . . Held, A. (2014). Land surface phenological response to decadal climate variability across Australia using satellite remote sensing. *Biogeosciences, 11*(18), 5181-5198.

Brovelli, M. A., Molinari, M. E., Hussein, E., Chen, J., & Li, R. (2015). The first comprehensive accuracy assessment of GlobeLand30 at a national level: methodology and results. *Remote Sensing, 7*(4), 4191-4212.

Cadavid, R. A., Yang, Y., McManus, D., Gray, D., Giraudoux, P., Barnes, T., . . . Clements, A. (2015). The landscape epidemiology of echinococcoses. *Infectious diseases of poverty, 5*(1), 13-13.

Caminade, C., Kovats, S., Rocklov, J., Tompkins, A. M., Morse, A. P., Colón-González, F. J., . . . Lloyd, S. J. (2014). Impact of climate change on global malaria distribution. *Proceedings of the National Academy of Sciences, 111*(9), 3286-3291.

Cao, L., Zhu, Y., Tang, G., Yuan, F., & Yan, Z. (2016). Climatic warming in China according to a homogenized data set from 2419 stations. *International Journal of Climatology*.

Cao, S., Chen, L., & Yu, X. (2009). Impact of China's Grain for Green Project on the landscape of vulnerable arid and semi-arid agricultural regions: a case study in northern Shaanxi Province. *Journal of Applied Ecology, 46*(3), 536-543.

Carpenter, S. R., DeFries, R., Dietz, T., Mooney, H. A., Polasky, S., Reid, W. V., & Scholes, R. J. (2006). Millennium Ecosystem Assessment: Research Needs. *Science, 314*(5797), 257-258.

Carreiras, J. M., Jones, J., Lucas, R. M., & Gabriel, C. (2014). Land Use and land cover change dynamics across the Brazilian Amazon: Insights from extensive time-series analysis of remote sensing data. *PloS one, 9*(8), e104144.

Cha, S.-y., & Park, C.-h. (2007). The utilization of Google Earth images as reference data for the multitemporal land cover classification with MODIS data of North Korea. *Korean Journal of Remote Sensing, 23*(5), 483-491.

Chen, H., Marter-Kenyon, J., López-Carr, D., & Liang, X.-y. (2015). Land cover and landscape changes in Shaanxi Province during China’s Grain for Green Program (2000–2010). *Environmental Monitoring and Assessment, 187*(10), 1-14. doi: 10.1007/s10661-015-4881-z

Chen, J., Chen, J., Liao, A., Cao, X., Chen, L., Chen, X., . . . Mills, J. (2015). Global land cover mapping at 30 m resolution: A POK-based operational approach. *ISPRS Journal of Photogrammetry and Remote Sensing, 103*, 7-27. doi: http://dx.doi.org/10.1016/j.isprsjprs.2014.09.002

Colón-González, F. J., Fezzi, C., Lake, I. R., & Hunter, P. R. (2013). The effects of weather and climate change on dengue. *PLoS Negl Trop Dis, 7*(11), e2503.

de Noblet-Ducoudré, N., Boisier, J.-P., Pitman, A., Bonan, G., Brovkin, V., Cruz, F., . . . Lawrence, P. (2012). Determining robust impacts of land-use-induced land cover

changes on surface climate over North America and Eurasia: results from the first set of LUCID experiments. *Journal of Climate, 25*(9), 3261-3281.
Department of the Interior - The United States Geological Survey (USGS). (2016a). Landsat 4-7 Climate Data Record (CDR) Surface Reflectance, Version 6.4. Product Guide Retrieved 2 May 2016, from http://landsat.usgs.gov/documents/cdr_sr_product_guide.pdf
Department of the Interior - The United States Geological Survey (USGS). (2016b). Provisional Landsat 8 Surface Reflectance Product. Retrieved 2 May 2016, from http://landsat.usgs.gov/documents/provisional_l8sr_product_guide.pdf
DIVA GIS. DIVA-GIS: Free, simple & Effective. Retrieved 25 November 2015, from http://www.diva-gis.org/
Dong, J., Xiao, X., Sheldon, S., Biradar, C., Zhang, G., Duong, N. D., . . . Moore III, B. (2014). A 50-m forest cover map in Southeast Asia from ALOS/PALSAR and its application on forest fragmentation assessment. *PloS one, 9*(1), e85801.
Environmental Systems Research Institute (ESRI). (2015). ArcGIS Software version 10.3.1. Redlands. California. from http://www.esri.com/software/arcgis/arcgis-for-desktop
Exelis Visual Information Solutions, I. (2015). ENVI software version 5.3. Boulder, CO, USA.
Fan, X., Ma, Z., Yang, Q., Han, Y., Mahmood, R., & Zheng, Z. (2015). Land use/land cover changes and regional climate over the Loess Plateau during 2001–2009. Part I: observational evidence. *Climatic Change, 129*(3-4), 427-440.
Foley, J. A., DeFries, R., Asner, G. P., Barford, C., Bonan, G., Carpenter, S. R., . . . Gibbs, H. K. (2005). Global consequences of land use. *Science, 309*(5734), 570-574.
Fonte, C. C., Bastin, L., See, L., Foody, G., & Lupia, F. (2015). Usability of VGI for validation of land cover maps. *International Journal of Geographical Information Science, 29*(7), 1269-1291.
Foody, G. M. (2002). Status of land cover classification accuracy assessment. *Remote Sensing of Environment, 80*(1), 185-201. doi: http://dx.doi.org/10.1016/S0034-4257(01)00295-4
Giraudoux, P., Raoul, F., Pleydell, D., Li, T., Han, X., Qiu, J., . . . Craig, P. S. (2013). Drivers of Echinococcus multilocularis transmission in China: small mammal diversity, landscape or climate? *PLoS Negl Trop Dis, 7*(3), e2045.
González, C., Paz, A., & Ferro, C. (2014). Predicted altitudinal shifts and reduced spatial distribution of Leishmania infantum vector species under climate change scenarios in Colombia. *Acta tropica, 129*, 83-90.
Google Inc. Panoramio. Photos of the world. 16 February 2016, from http://www.panoramio.com/
Google Inc. (2015). Google Earth Pro version 7.1.5.1557. Retrieved 25 January 2016, from https://www.google.com.au/earth/
Goslee, S. C. (2011). Analyzing remote sensing data in R: the landsat package. *Journal of Statistical Software, 43*(4), 1-25.
Hamm, N. A., Magalhães, R. J. S., & Clements, A. C. (2015). Earth Observation, Spatial Data Quality, and Neglected Tropical Diseases. *PLoS Negl Trop Dis, 9*(12), e0004164.
Hu, Q., Wu, W., Xia, T., Yu, Q., Yang, P., Li, Z., & Song, Q. (2013). Exploring the use of Google Earth imagery and object-based methods in land use/cover mapping. *Remote Sensing, 5*(11), 6026-6042.
Hu, Y., Zhang, Z., Chen, Y., Wang, Z., Gao, J., Tao, B., . . . Jiang, Q. (2013). Spatial pattern of schistosomiasis in Xingzi, Jiangxi Province, China: the effects of environmental factors. *Parasites & vectors, 6*(1), 1.

Ingram, J., Ericksen, P., & Liverman, D. (2012). *Food security and global environmental change*: Routledge.

Japan Aerospace Exploration Agency (JAXA). Global 25m Resolution PALSAR-2/PALSAR Mosaic and Forest/Non-Forest Map. Retrieved 25 February 2016, from http://www.eorc.jaxa.jp/ALOS/en/palsar_fnf/data/index.htm

Japan Aerospace Exploration Agency (JAXA), & Earth Observation Research Center (EORC). Global 25m Resolution PALSAR-2/PALSAR Mosaic and Forest/Non-Forest Map (FNF). Dataset Description. Retrieved 25 February 2016, from http://www.eorc.jaxa.jp/ALOS/en/palsar_fnf/DatasetDescription_PALSAR2_Mosaic_FNF_revA.pdf

Jokar Arsanjani, J., See, L., & Tayyebi, A. (2016). Assessing the suitability of GlobeLand30 for mapping land cover in Germany. *International Journal of Digital Earth*, 1-19.

Jokar Arsanjani, J., Tayyebi, A., & Vaz, E. (2016). GlobeLand30 as an alternative fine-scale global land cover map: Challenges, possibilities, and implications for developing countries. *Habitat International, 55*, 25-31. doi: http://dx.doi.org/10.1016/j.habitatint.2016.02.003

Jones, P. D., New, M., Parker, D. E., Martin, S., & Rigor, I. G. (1999). Surface air temperature and its changes over the past 150 years. *Reviews of Geophysics, 37*(2), 173-199.

Kalnay, E., & Cai, M. (2003). Impact of urbanization and land-use change on climate. *Nature, 423*(6939), 528-531.

Lambin, E. F., Turner, B. L., Geist, H. J., Agbola, S. B., Angelsen, A., Bruce, J. W., . . . Folke, C. (2001). The causes of land-use and land-cover change: moving beyond the myths. *Global Environmental Change, 11*(4), 261-269.

Landis, J. R., & Koch, G. G. (1977). The Measurement of Observer Agreement for Categorical Data. *Biometrics, 33*(1), 159-174. doi: 10.2307/2529310

Lemmens, M. (2011). *Geo-information: technologies, applications and the environment* (Vol. 5): Springer Science & Business Media.

Li, J., Zheng, G., Liu, H., Wang, L., Tang, Z., Shi, H., . . . Wang, H. Situation Analysis of Ningxia Province. *China Climate Change Partnership Framework - Enhanced strategies for climate-proofed and environmentally sound agricultural production in the Yellow River Basin (C-PESAP).* Retrieved 22 March 2016, from http://www.fao.org/fileadmin/templates/cpesap/Data/Ningxia/SASNingxiawp.pdf

Li, Y., Conway, D., Wu, Y., Gao, Q., Rothausen, S., Xiong, W., . . . Lin, E. (2013). Rural livelihoods and climate variability in Ningxia, Northwest China. *Climatic Change, 119*(3-4), 891-904.

Lillesand, T., Kiefer, R. W., & Chipman, J. (2014). *Remote sensing and image interpretation*: John Wiley & Sons.

Liu, J., & Diamond, J. (2005). China's environment in a globalizing world. *Nature, 435*(7046), 1179-1186.

Liu, J., Kuang, W., Zhang, Z., Xu, X., Qin, Y., Ning, J., . . . Yan, C. (2014). Spatiotemporal characteristics, patterns, and causes of land-use changes in China since the late 1980s. *Journal of Geographical Sciences, 24*(2), 195-210.

Liu, J., Li, S., Ouyang, Z., Tam, C., & Chen, X. (2008). Ecological and socioeconomic effects of China's policies for ecosystem services. *Proceedings of the National Academy of Sciences, 105*(28), 9477-9482.

Lu, N., Hernandez, A. J., & Ramsey, R. D. (2015). Land cover dynamics monitoring with Landsat data in Kunming, China: a cost-effective sampling and modelling scheme using Google Earth imagery and random forests. *Geocarto International, 30*(2), 186-201.

Manakos, I., Chatzopoulos-Vouzoglanis, K., Petrou, Z. I., Filchev, L., & Apostolakis, A. (2014). Globalland30 mapping capacity of land surface water in Thessaly, Greece. *Land, 4*(1), 1-18.

MRC Biostatistics Unit. (2014). The BUGS Project. OpenBUGs. Version 3.2.3 rev 1012. Cambridge, UK., from http://www.mrc-bsu.cam.ac.uk/software/bugs/

National Bureau of Statistics of China. (2014). China Statistical Year Book 2014. Population and its composition. Retrieved 2 June 2016, from http://www.stats.gov.cn/tjsj/ndsj/2014/indexeh.htm

National Geomatics Center of China. (2014). GlobeLand30. A 30-meter Global Land Cover Dataset. Retrieved 12 December 2015, from http://glc30.tianditu.com/

Newbold, T., Hudson, L. N., Hill, S. L., Contu, S., Lysenko, I., Senior, R. A., . . . Collen, B. (2015). Global effects of land use on local terrestrial biodiversity. *Nature, 520*(7545), 45-50.

Peng, X. (2011). China’s demographic history and future challenges. *Science, 333*(6042), 581-587.

Pielke, R. A. (2005). Land Use and Climate Change. *Science, 310*(5754), 1625-1626.

Pielke, R. A., Marland, G., Betts, R. A., Chase, T. N., Eastman, J. L., Niles, J. O., & Running, S. W. (2002). The influence of land-use change and landscape dynamics on the climate system: relevance to climate-change policy beyond the radiative effect of greenhouse gases. *Philosophical Transactions of the Royal Society of London A: Mathematical, Physical and Engineering Sciences, 360*(1797), 1705-1719.

Pleydell, D. R., Yang, Y. R., Danson, F. M., Raoul, F., Craig, P. S., McManus, D. P., . . . Giraudoux, P. (2008). Landscape composition and spatial prediction of alveolar echinococcosis in southern Ningxia, China. *PLoS Negl Trop Dis, 2*(9), e287.

Qi, Y., Wang, Y., & Wang, J. (2003). *Ningxia land cover change and its driving factors during past decade.* Paper presented at the Third International Asia-Pacific Environmental Remote Sensing Remote Sensing of the Atmosphere, Ocean, Environment, and Space.

Raj, R., Hamm, N. A., & Kant, Y. (2013). Analysing the effect of different aggregation approaches on remotely sensed data. *International journal of remote sensing, 34*(14), 4900-4916.

RStudio Team. (2014). RStudio: Integrated Development for R. RStudio, Inc., Boston, MA., from http://www.rstudio.com/.

Sala, O. E., Chapin, F. S., Armesto, J. J., Berlow, E., Bloomfield, J., Dirzo, R., . . . Wall, D. H. (2000). Global Biodiversity Scenarios for the Year 2100. *Science, 287*(5459), 1770-1774.

Sawaya, K. E., Olmanson, L. G., Heinert, N. J., Brezonik, P. L., & Bauer, M. E. (2003). Extending satellite remote sensing to local scales: land and water resource monitoring using high-resolution imagery. *Remote Sensing of Environment, 88*(1), 144-156.

Shalaby, A., & Tateishi, R. (2007). Remote sensing and GIS for mapping and monitoring land cover and land-use changes in the Northwestern coastal zone of Egypt. *Applied Geography, 27*(1), 28-41.

Shi, X., Nie, S., Ju, W., & Yu, L. (2016). Application and impacts of the GlobeLand30 land cover dataset on the Beijing Climate Center Climate Model. *IOP Conference Series: Earth and Environmental Science, 34*(1), 012032.

Statistical Bureau of Ningxia Hui Autonomous Region. (2014). Population Ningxia 2014. Retrieved 20 March 2016, from http://www.nxtj.gov.cn/nxtjjxbww/tjxx/201503/t20150310_52808.html

Strahler, A. H. (1980). The use of prior probabilities in maximum likelihood classification of remotely sensed data. *Remote Sensing of Environment, 10*(2), 135-163.

The National Aeronautics and Space Administration (NASA) and Ministry of Economy Trade and Industry (METI). (2011). The Advanced Spaceborne Thermal Emission and Reflection Radiometer (ASTER) Global Digital Elevation Model (GDEM). Version 2. ASTER GDEM is a product of NASA and METI
Retrieved 16 November 2015, from https://asterweb.jpl.nasa.gov/gdem.asp

The United States Geological Survey (USGS). EarthExplorer. Retrieved 14 June 2015, from http://earthexplorer.usgs.gov/

The University of Nottingham. China Policy Institute. (2010). "Grain for Green Programme" in China: policy making and implementation?. Briefing series. Issue 60. Retrieved 2 June 2016, from http://www.nottingham.ac.uk/cpi/documents/briefings/briefing-60-reforestation.pdf

Turner, B. L., Lambin, E. F., & Reenberg, A. (2007). The emergence of land change science for global environmental change and sustainability. *Proceedings of the National Academy of Sciences, 104*(52), 20666-20671.

Turner, I., Moss, R., & Sz Skole, D. D., 1993. Relating land use and global land-cover change: a proposal for an IGBP–HDP core project. *Report from the IGBP-HDP Working Group on land use/land-cover change. Joint publication of the International Geosphere-Biosphere Programme (Report No. 24) and the Human Dimensions of Global Environmental Change Programme (Report No. 5). Stockholm: Royal Swedish Academy of Science*.

Verburg, P. H., Van De Steeg, J., Veldkamp, A., & Willemen, L. (2009). From land cover change to land function dynamics: a major challenge to improve land characterization. *Journal of environmental management, 90*(3), 1327-1335.

Vitousek, P. M., Mooney, H. A., Lubchenco, J., & Melillo, J. M. (1997). Human domination of Earth's ecosystems. *Science, 277*(5325), 494-499.

Walker, W. S., Stickler, C. M., Kellndorfer, J. M., Kirsch, K. M., & Nepstad, D. C. (2010). Large-area classification and mapping of forest and land cover in the Brazilian Amazon: a comparative analysis of ALOS/PALSAR and Landsat data sources. *Selected Topics in Applied Earth Observations and Remote Sensing, IEEE Journal of, 3*(4), 594-604.

Wang, C., Yang, Y., & Zhang, Y. (2011). Economic Development, Rural livelihoods, and Ecological Restoration: Evidence from China. *Ambio, 40*(1), 78-87. doi: 10.1007/s13280-010-0093-5

Wang, X., Lu, C., Fang, J., & Shen, Y. (2007). Implications for development of grain-for-green policy based on cropland suitability evaluation in desertification-affected north China. *Land Use Policy, 24*(2), 417-424.

Wang, Y., Gao, J., Wang, J., & Qiu, J. (2014). Value assessment of ecosystem services in nature reserves in Ningxia, China: a response to ecological restoration. *PloS one*, *9*(2), e89174.

Weng, Q. (2002). Land use change analysis in the Zhujiang Delta of China using satellite remote sensing, GIS and stochastic modelling. *Journal of environmental management, 64*(3), 273-284.

Xin, Z., Xu, J., & Zheng, W. (2008). Spatiotemporal variations of vegetation cover on the Chinese Loess Plateau (1981–2006): Impacts of climate changes and human activities. *Science in China Series D: Earth Sciences, 51*(1), 67-78.

Yan-qiong, Y., Guo-jie, C., & Hong, F. (2003). Impacts of the “Grain for Green” project on rural communities in the Upper Min River Basin, Sichuan, China. *Mountain Research and Development, 23*(4), 345-352.

Yang, J., Tan, C., Wang, S., Wang, S., Yang, Y., & Chen, H. (2015). Drought Adaptation in the Ningxia Hui Autonomous Region, China: Actions, Planning, Pathways and Barriers. *Sustainability, 7*(11), 15029-15056.

Yu, L., Wang, J., Li, X., Li, C., Zhao, Y., & Gong, P. (2014). A multi-resolution global land cover dataset through multisource data aggregation. *Science China Earth Sciences, 57*(10), 2317-2329.

Yuan, F., Sawaya, K. E., Loeffelholz, B. C., & Bauer, M. E. (2005). Land cover classification and change analysis of the Twin Cities (Minnesota) Metropolitan Area by multitemporal Landsat remote sensing. *Remote Sensing of Environment*, *98*(2), 317-328.

Zhang, L., Tu, Q., & Mol, A. P. (2008). Payment for environmental services: The sloping land conversion program in Ningxia autonomous region of China. *China & World Economy, 16*(2), 66-81.

Zhao, X., Lv, X., & Dai, J. (2010). Impact assessment of the "Grain for Green Project" and discussion on the development models in the mountain-gorge regions. *Frontiers of Earth Science in China, 4*(1), 105-116.

Zhou, D., Zhao, S., & Zhu, C. (2012). The Grain for Green Project induced land cover change in the Loess Plateau: a case study with Ansai County, Shanxi Province, China. *Ecological indicators*, *23*, 88-94.